Acoustically Mounted Microcrystals Yield High Resolution X-ray Structures[†‡]

Alexei S. Soares,[1*] Matthew A. Engel,[2,3] Richard Stearns,[4] Sammy Datwani,[4] Joe Olechno,[4] Richard Ellson,[4] John M. Skinner,[1] Marc Allaire,[2*] and Allen M. Orville[1*]

[1] Biology Department, Brookhaven National Laboratory, Upton NY 11973-5000

[2] National Synchrotron Light Source, Brookhaven National Laboratory, Upton NY 11973-5000

[3] Department of Biomedical Engineering, Stony Brook University, Stony Brook, NY 11794-2580

[4] Labcyte Inc. 1190 Borregas Avenue, Sunnyvale, California 94089

[*] For information please contact:

ASS, Phone: 631-344-7306; Fax: 631-344-2741; E-mail: soares@bnl.gov

MA, Phone: 631-344-4795; Fax: 631-344-3238; E-mail: allaire@bnl.gov

AMO, Phone: 631-344-4739; Fax: 631-344-2741; E-mail: amorv@bnl.gov

AUTHOR CONTRIBUTIONS:

ASS, MA, and AMO designed the experiments. ASS, MAE and MA performed crystallization experiments. ASS, MAE, RE, JO, RS and SD performed the acoustic droplet ejection experiments. ASS, MAE, JMS, and MA collected the X-ray diffraction data. ASS, MAE, MA and AMO analyzed the data. AMO, ASS, and MA wrote the manuscript.

COMPETING FINANCIAL STATEMENT:

ASS, MAE, JMS, MA and AMO declare no competing financial interests. RE (chief technology officer), RS (principal scientist), JO (vice president of business development and strategic marketing), and SD (director of chemistry and senior staff engineer) are employed by Labcyte. RE, RS, JO, and SD either hold stock or stock options for Labcyte. Patents have been issued, or are pending, related to acoustic droplet ejection technology to Labcyte.

Supplementary section 1 – Insulin microcrystal preparation

Insulin for crystallization was obtained from Sigma-Aldrich[®] and used without further purification. The protein forms well diffracting crystals in space group $R3$, $a = b = 82.5$ Å, $c = 34.1$ Å, $\alpha = \beta = 90°$, $\gamma = 120°$. The microcrystals were grown by dissolving porcine insulin in the following low-salt crystallizing solution: 25 mg insulin, 200 µl 0.02M HCl, 100 µl 0.20 M sodium citrate, 60 µl acetone, 20 µl H_2O and 20 µl 0.12M $ZnSO_4$, pH 6.8. The protein solubility increases with increasing temperature. Therefore, the crystal nucleation rate and the final crystal size obtained is manipulated by controlling the rate at which the preparation cools from 313 K down to 293 K .(*1*) This process yields high quality crystals with mono-disperse sizes (Supplementary Fig. 1). Slurries of insulin microcrystals were cryoprotected in bulk by adding 1.2M trehalose to the mother liquor-crystal slurry. The flat rhombohedra-shaped crystals had two roughly equal long axes, and a much smaller third axis (Supplementary Fig. 2). For convenience, the slurries of microcrystals were partitioned into four groups according to the average crystal size. Crystals in the first group were small (~5 µm long axes), the second were intermediate sized (~10 µm), the third were large sized (~20 µm), and the last group had all three sizes mixed together. Crystals were spun down under light centrifugation (1000 rpm setting on a table top centrifuge, corresponding to ~45 g) and the supernatant was removed until the volume of the crystal pellet approximately equaled the remaining volume of mother liquor. ADE mounted crystals were transferred from the source wells, onto MiTeGen[TM] micromeshes, and flash-cooled by plunging them directly into liquid nitrogen.

Supplementary section 2 - Lysozyme microcrystal preparation

Hen egg white lysozyme was obtained from Sigma-Aldrich and used without further purification. It forms crystals on the order of ~5-20 µm that can be grown by creating a supersaturated solution containing high concentrations of protein and precipitant.(*2*) Crystals were grown by combining 200 µl of hen egg-white lysozyme protein solution (200 mg/ml lysozyme in 0.1 M NaAcetate pH 4.5) with 200 µl of high-salt crystallizing solution containing glycerol (0.1 M NaAcetate pH 4.5, 1.0M NaCl, and 50% glycerol) in a microcentrifuge tube, sealing it with Parafilm M[TM] film and placing the mixture on a rocker overnight. Crystals (space group $P4_32_12$, $a = b = 80.2$ Å, $c = 37.7$ Å, $\alpha = \beta = \gamma = 90°$) generally formed within one hour after mixing (Supplementary Fig. 3). Continuous rocking impedes the growth of large single

crystals or amorphous aggregates. Solutions containing crystals were removed from the rocker and allowed to stand for several minutes, during which the majority of crystals settled to the bottom of the microcentrifuge tube. Solutions for ADE and hand mounting were selected from the supernatant because it contained a lower density of crystals and a higher concentration of microcrystals. The supernatant was divided into two parts; one part was for control samples, which were hand mounted, and the second part was for ADE mounted samples. Both control and ADE samples were prepared on MiTeGen micromeshes and flash-cooled by plunging them into liquid nitrogen.

Supplementary section 3 – Crystal screening software, phasing and model refinement

We and others(*3*) have developed a raster-scan software system to scan MiTeGen micromeshes by dividing each mesh into a grid of M by N arbitrarily sized fields (see Fig. 1c in the main paper). Each field is screened for X-ray diffraction and rapidly evaluated by DISTL(*4*) or by the EDNA(*5*) software packages. Data collection parameters for fields which test positive for a diffracting specimen are determined either by the user or by software. Comprehensive meta-data output from screening and data collection software are automatically deposited into our PXDB database.(*6*)

X-ray diffraction data were integrated and reduced with HKL2000(*7*) and further handled with the CCP4 suite of programs.(*8*) Molecular replacement solutions using polyalanine starting models were very easy to obtain from acoustically prepared insulin crystals and from acoustically prepared lysozyme crystals. The starting models were generated by importing the known structures into coot (protein data bank entries 4ins and 3ijv), removing all water molecules, and mutating all side chains to alanines. Each data set was phased by MOLREP(*9*) using this starting model. The side chains easily settled into the resulting difference electron density maps using COOT(*10*). REFMAC(*11*) and on ARP/WARP(*12, 13*) were iteratively used to refine each model. RMS coordinate errors of the refined models relative to the published models of the insulin structure (4ins) and lysozyme structure (3ijv) were 0.25 Å (10 µm insulin), 0.28 Å (20 µm insulin), and 0.47 Å (lysozyme).

Zinc is a robust anomalous scatterer, but when it is located on a symmetry axis as in rhombohedral insulin, it yields a map that cannot be better than the superposition of the true map and the inverse hand map. Any significant experimental noise in the data will result in failure of

solvent flattening and a poorly-defined electron density map.   For this reason, the anomalous signal from the two zinc atoms on the 3-fold axis of the insulin hexamer has previously been used to test new methods. To test the resilience of the anomalous signal after combining multiple data sets from acoustically prepared micro crystals, we merged anomalous data from nine ADE prepared 20 μm crystals and solved the structure using the SAD method. SHELXD(*14*) was used to identify the two zinc atoms on the three fold axis. PHASER(*15*) yielded an initial map that was readily interpretable in the vicinity of the anti-parallel beta strands B23-B28 and D23-D28 (see Figure 2a in the main paper). The two hexapeptides were manually positioned using coot, and placed in sequence by the Phe-Phe-Tyr residues. PHENIX(*16*) used the two hexapeptide partial model in combination with the anomalous signal to build 74 out of 102 residues. The model was then completed iteratively using COOT and PHASER, and refined using REFMAC and ARP/WARP solvent.

Supplementary section 4 - ADE transfer of microcrystals

We used a "Sequoia" instrument, which consists of a modified Echo® Liquid Handling System with all components accessible on a bread-board support, with central computer control from a remote electronics rack. The Sequoia also features an on-axis optical system and camera located above the transducer. A perpendicular off-axis optical system is equipped with a stroboscopic camera so that the position and velocity of each ejection is optically determined. When the acoustic wave is focused within the main volume of the source well, the resulting transfer of kinetic energy agitates and mixes the source well. Acoustic energy that is not transferred to the liquid is returned to the transducer as an audible echo. This provides a means to monitor the volume of the source well in real time. Standard MiTeGen micromeshes were positioned above the transducer and aligned with a dial micrometer. After samples were transferred to the micromesh, they were quickly plunged into liquid nitrogen and stored at 77 K until X-ray diffraction data was collected.

The lysozyme crystals tended to settle to the bottom of the source well, which prevented their transfer with the ejected droplets because the acoustic propulsion occurs very near the surface. Consequently, we intentionally focused the acoustic energy into the body of the source

well to mix it just prior to the ejection pulse. This distributed the crystals more evenly throughout the well volume and resulted in transfer of lysozyme crystals.

The insulin crystals settled slowly to the bottom because the density of the mother liquor augmented with trehalose almost matches that of the crystals. We explored the possibility of using surface depletion due to settling to selectively eject small crystals from a mixed insulin batch. As expected, we observed that after allowing the mixed batch to stand for 15 minutes, only small crystals remained near the surface. When a droplet was then ejected from the surface, it contained only small crystals.

An additional difficulty was encountered when ejecting crystals from the mixed insulin batch. When the transducer wavelength approaches the size of suspended particles, there is a substantial increase in diffractive dissipation of the acoustic signal. When dispensing from a mono-disperse source well this phenomenon did not occur because the desired droplet size is always moderately larger than the specimen size. However, having a very high density of mixed size specimens resulted in an observable attenuation of the amplitude of the incident sound wave for many desirable frequency settings. It was possible to overcome this problem by increasing the power setting on the transducer, without any observed deleterious effect on the diffraction data of the transferred samples. Furthermore, particulate matter in the well perturbs the sound waves by shifting the focus of the acoustic energy. However, we were unable to cause a failure of transfer with either small glass shards or denatured protein particulates.

References

1.	Soares, A. S., Caspar, D. L., Weckert, E., Heroux, A., Holzer, K., Schroer, K., Zellner, J., Schneider, D., Nolan, W., and Sweet, R. M. (2003) Three-beam interference is a sensitive measure of the efficacy of macromolecular refinement techniques, *Acta Crystallogr D Biol Crystallogr 59*, 1716-1724.
2.	Allaire, M., Moiseeva, N., Botez, C. E., Engel, M. A., and Stephens, P. W. (2009) On the possibility of using polycrystalline material in the development of structure-based generic assays, *Acta Crystallogr D Biol Crystallogr 65*, 379-382.
3.	Cherezov, V., Hanson, M. A., Griffith, M. T., Hilgart, M. C., Sanishvili, R., Nagarajan, V., Stepanov, S., Fischetti, R. F., Kuhn, P., and Stevens, R. C. (2009) Rastering strategy for screening and centring of microcrystal samples of human membrane proteins with a sub-10 mu m size X-ray synchrotron beam, *J R Soc Interface 6*, S587-S597.
4.	Zhang, Z., Sauter, N. K., van den Bedem, H., Snell, G., and Deacon, A. M. (2006) Automated diffraction image analysis and spot searching for high-throughput crystal screening, *Journal of Applied Crystallography 39*, 112-119.

5.   Incardona, M. F., Bourenkov, G. P., Levik, K., Pieritz, R. A., Popov, A. N., and Svensson, O. (2009) EDNA: a framework for plugin-based applications applied to X-ray experiment online data analysis, *J Synchrotron Radiat 16*, 872-879.

6.   Skinner, J. M., Cowan, M., Buono, R., Nolan, W., Bosshard, H., Robinson, H. H., Heroux, A., Soares, A. S., Schneider, D. K., and Sweet, R. M. (2006) Integrated software for macromolecular crystallography synchrotron beamlines II: revision, robots and a database, *Acta Crystallogr D Biol Crystallogr 62*, 1340-1347.

7.   Otwinowski, Z., and Minor, W. (1997) Processing of X-ray diffraction data collected in oscillation mode, *Method Enzymol 276*, 307-326.

8.   4, C. C. P. N. (1994) The CCP4 suite: programs for protein crystallography, *Acta Crystallogr D Biol Crystallogr 50*, 760-763.

9.   Vagin, A., and Teplyakov, A. (1997) MOLREP: an Automated Program for Molecular Replacement, *Journal of Applied Crystallography 30*, 1022-1025.

10.   Emsley, P., and Cowtan, K. (2004) Coot: model-building tools for molecular graphics, *Acta Crystallogr D Biol Crystallogr 60*, 2126-2132.

11.   Winn, M. D., Murshudov, G. N., and Papiz, M. Z. (2003) Macromolecular TLS refinement in REFMAC at moderate resolutions, *Methods Enzymol 374*, 300-321.

12.   Langer, G., Cohen, S. X., Lamzin, V. S., and Perrakis, A. (2008) Automated macromolecular model building for X-ray crystallography using ARP/wARP version 7, *Nat Protoc 3*, 1171-1179.

13.   Morris, R. J., Perrakis, A., and Lamzin, V. S. (2003) ARP/wARP and automatic interpretation of protein electron density maps, *Methods Enzymol 374*, 229-244.

14.   Schneider, T. R., and Sheldrick, G. M. (2002) Substructure solution with SHELXD, *Acta Crystallogr D Biol Crystallogr 58*, 1772-1779.

15.   McCoy, A. J., Grosse-Kunstleve, R. W., Adams, P. D., Winn, M. D., Storoni, L. C., and Read, R. J. (2007) Phaser crystallographic software, *J Appl Crystallogr 40*, 658-674.

16.   Adams, P. D., Afonine, P. V., Bunkoczi, G., Chen, V. B., Davis, I. W., Echols, N., Headd, J. J., Hung, L. W., Kapral, G. J., Grosse-Kunstleve, R. W., McCoy, A. J., Moriarty, N. W., Oeffner, R., Read, R. J., Richardson, D. C., Richardson, J. S., Terwilliger, T. C., and Zwart, P. H. (2010) PHENIX: a comprehensive Python-based system for macromolecular structure solution, *Acta Crystallogr D Biol Crystallogr 66*, 213-221.

Table S1. Data collection and model refinement statistics

	Insulin (10 μm)	Insulin (20 μm)	Lysozyme (20 μm)
X-ray Diffraction Data Collection			
# of crystals	14	9	2
X-ray source	NSLS X25	NSLS X25	APS 23ID-D
Wavelength (Å)	1.280	1.280	1.000
Beam size (μm)	20 x 20	20 x 20	10 x 10
Space group	$R3$	$R3$	$P4_32_12$
Unit cell dimensions			
a, b, c (Å)	81.7, 81.7, 33.9	81.7, 81.7, 33.9	79.3, 79.3, 36.9
α β γ (°)	90, 90, 120	90, 90, 120	90, 90, 90
Resolution (Å)	50 - 1.9	50 - 1.8	30 - 1.8
R_{sym} or R_{merge}	24.0 (39.6) [a]	11.4 (61.6) [a]	10.9 (36.7) [a]
$I / \sigma I$	46.4 (3.4) [a]	62.2 (2.1) [a]	16.9 (1.2) [a]
Complete (%)	93.5 (58.7) [a]	99.8 (96.7) [a]	94.9 (62.5) [a]
Redundancy	6.5	10.5	1.8
Model Refinement			
# Reflections	5917	7398	10280
R_{work} / R_{free}	16.7 / 20.3	18.3 / 22.0	16.8 / 21.2
# Atoms	845	857	1111
Protein	804	804	1000
Ligand / ion	2	2	0
Water	39	51	111
B-factors			
Protein	40.4	37.3	19.4
Ligand / ion	33.9	30.4	-
Water	49.4	47.2	29.1
R.m.s. deviations in bond			
Distances (Å)	0.025	0.025	0.021
Angles (°)	2.244	2.159	1.938

[a] Highest resolution shell
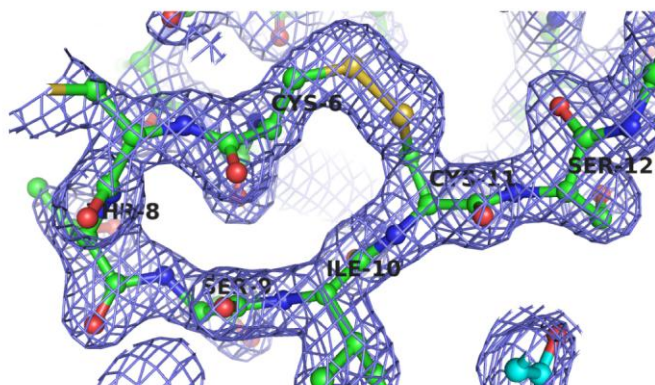
Figure S1: The final electron density map to 1.8Å resolution (2Fo – Fc, contoured at 1 σ) from the X-ray diffraction dataset merged from nine ADE-mounted insulin microcrystals shown in figure 1b. The region of the Cys6-Cys11 disulfide bridge in chain A of the protein is shown with C, N, O, and S atoms rendered in green, blue, red and gold, respectively. The cyan-colored C atoms are from an adjacent subunit.
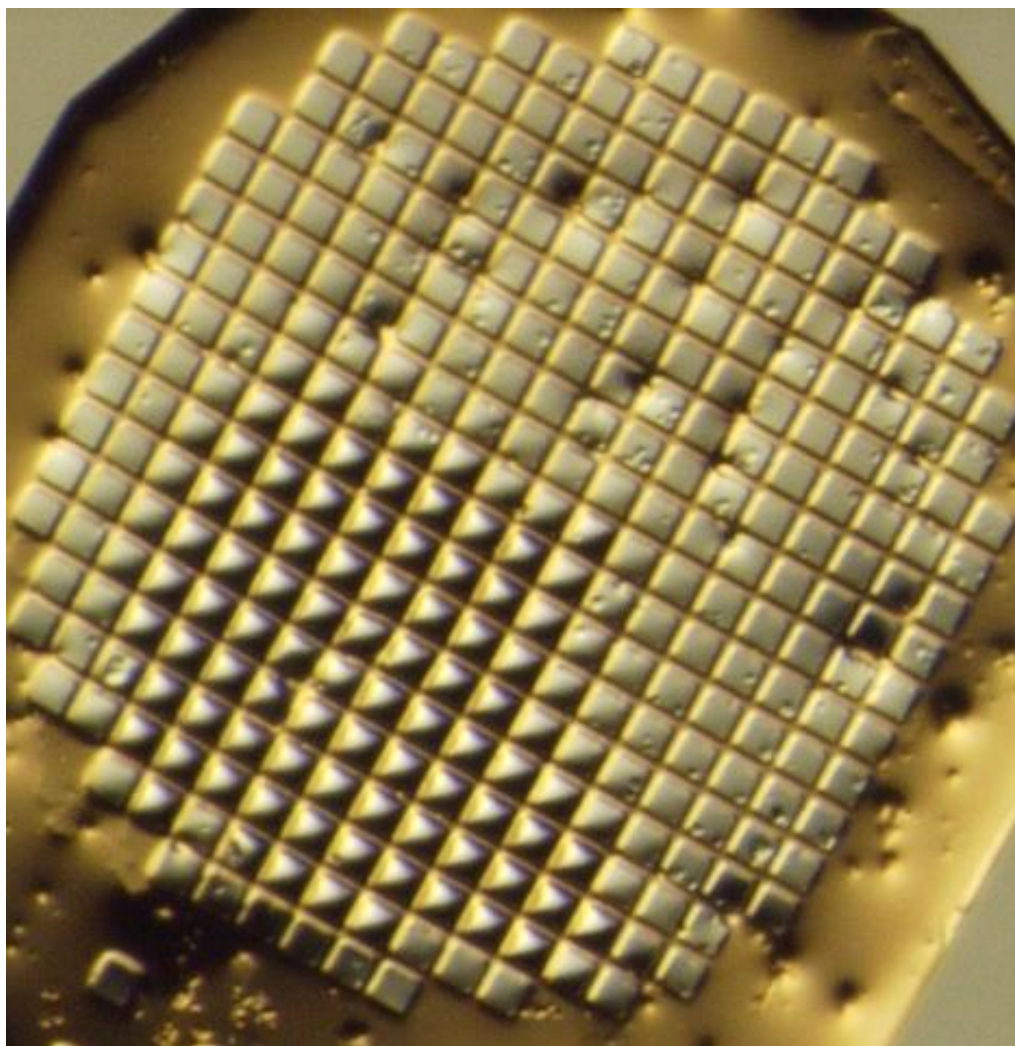
Figure S2 – Monodisperse insulin microcrystals

Control of the crystallization conditions resulted in crystals of uniform size. The grid-spacing of this MiTeGen 400/25 micromesh is 25 μm x 25 μm. Visual inspection of this field of view determined that the microcrystals had a mean size of 5.2 μm with a variance of only 1.5 μm.
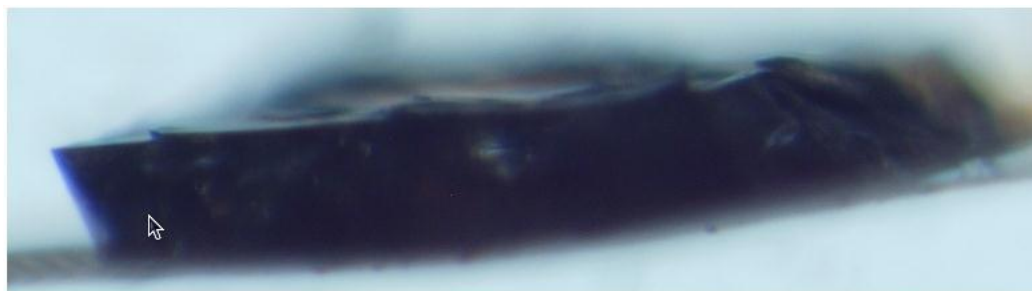
Figure S3 – Insulin crystal geometry

Orthogonal views of a large (~300 µm x ~300 µm x ~70 µm), insulin crystal with side length ratios of ~4:4:1 illustrates the crystal morphology observed for macro- and microcrystals.
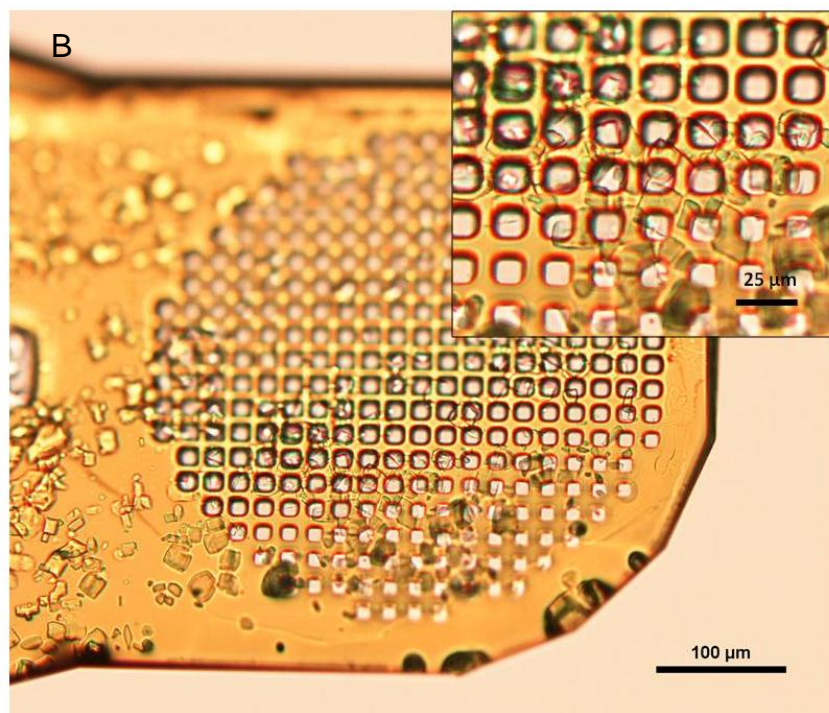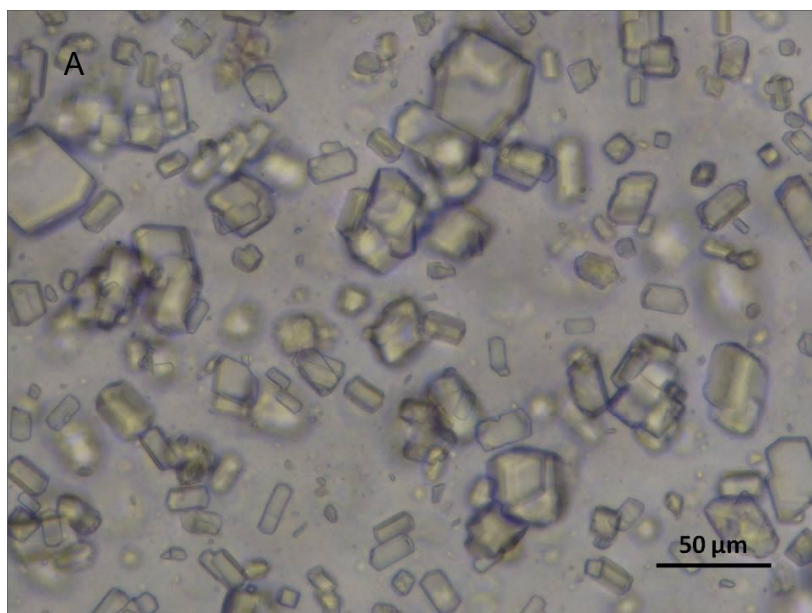
Figure S4 – Lysozyme microcrystal slurries

Lysozyme crystals (A) grew within one hour after mixing precipitant and protein solutions as described in the text. (B) Samples were mounted onto MiTeGen micromeshes with a mesh opening of 10 µm immediately prior to cryocooling.